# Low RF-Complexity Massive MIMO Systems Based on Vertical Spatial Filtering for Urban Macro Cellular Networks

Xiaolei Jiang, *Member, IEEE*, Han Wang, Zhijun Zhang, *Fellow, IEEE*, Xinyu Gao, *Student Member, IEEE*, Linglong Dai, *Senior Member, IEEE*, and Magdy F. Iskander, *Life Fellow, IEEE*

***Abstract*—In this paper, we consider a massive multiple-input multiple-output (MIMO) system for urban macro cellular networks. A new technique named vertical spatial filtering (VSF) is proposed to achieve low radio frequency (RF) complexity by exploiting the spatial beam redundancy in elevation domain. Specifically, VSF consists of two parts: beam mapping and beam selection. We first adopt beam mapping to transform the received signals from antenna space into beam space. Then, we use beam selection to pick out part of the RF chains so as to realize the reduction of RF complexity. A three-dimensional channel model is adopted to evaluate the system performance. Two strategies for beam selection are proposed and numerical results are presented. The results show that the reduced system with VSF has the performance comparable to the complete system, while only a small amount of RF chains is required in vertical dimension of the two-dimensional base station array.**

***Index Terms*—Massive multiple-input multiple-output (MIMO), multi-user system, radio frequency (RF) beamforming, RF complexity, vertical spatial filtering (VSF).**

## I. Introduction

MULTIPLE-INPUT multiple-output (MIMO) technology has been actively and intensively investigated over the past years [1]. Some standards-driven commercial wireless networks like the fourth generation (4G) mobile telecommunications [2], [3] have already successfully adopted MIMO technology in practical systems. Spatial multiplexing is a key advantage offered by MIMO technology, which allows multiple independent data streams to be transmitted simultaneously by multiple transmit antennas, thereby directly improving the channel capacity. More recently, massive MIMO, also known as large-scale antenna system or full-dimension MIMO, has emerged as a promising key technology for the fifth generation (5G) mobile telecommunications [4], [5]. Massive MIMO entails hundreds of antennas at the base station (BS), and such a scaling up effect will bring some new opportunities that cannot be found in conventional MIMO systems, e.g., extremely low power for each antenna element that enables much higher energy efficiency, much higher spectral efficiency that can be achieved by extra degree of freedom in the spatial domain, and the asymptotical orthogonality among user channels that makes simple linear signal processing techniques near optimal [6]. However, challenges are co-existing with the opportunities at the present stage [6], [7]. There are still many open issues that need further investigation for massive MIMO. One key problem is that each transmit antenna requires one specific radio frequency (RF) chain, including up/down converters, analog-to-digital (A/D)-digital-to analog (D/A) converters and so forth, which makes the whole massive MIMO system very complex and expensive when the number of BS antennas is huge.

To alleviate the RF-complexity of MIMO system, several approaches have already been proposed in recent years. Antenna selection [8]–[10] is an efficient solution to select $L$ out of $N$ ($L < N$) antennas for signal transmission, so as to reduce the required number of RF chains. Spatial modulation [11]–[13] is a more ambitious solution that antenna patterns can be also used to transmit extra bits, in which only one RF chain is required. While generalized spatial modulation [14]–[16], which can be implemented by either encoding the information into combinations of antennas or by activating more than one RF chain and amalgamating spatial modulation with spatial multiplexing, allows the designer to identify the number of active RF chains depending on the complexity, power consumption and spectral efficiency of interest. The energy efficiency of spatial modulation is much higher than that of conventional MIMO system, but it comes at the expense of sacrificing spectrum efficiency. However, spatial modulation is an attractive compromise between energy efficiency and spectrum efficiency. A hybrid analog and digital precoding scheme is proposed in millimeter wave (mmWave) MIMO system [17]. By leveraging the limited scattering nature of mmWave channels, a low hardware-complexity solution can be realized.

Manuscript received October 16, 2016; revised March 27, 2017; accepted May 22, 2017. Date of publication June 5, 2017; date of current version October 13, 2017. This work was supported in part by the National Natural Science Foundation of China under Contract 61525104 and in part by the Keysight Technologies, Inc. The review of this paper was coordinated by Prof. S. Tomasin. *(Corresponding author: Zhijun Zhang.)*

X. Jiang, H. Wang, Z. Zhang, X. Gao, and L. Dai are with Tsinghua National Laboratory for Information Science and Technology, Department of Electronic Engineering, Tsinghua University, Beijing 100084, China (e-mail: jiangxiaolei3@huawei.com; wanghanatbupt@gmail.com; zjzh@tsinghua.edu.cn; gxy1231992@sina.com; daill@tsinghua.edu.cn).

M. F. Iskander is with Hawaii Center for Advanced Communication, University of Hawaii at Manoa, Honolulu, HI 96822 USA (e-mail: iskander@spectra.eng.hawaii.edu).

Color versions of one or more of the figures in this paper are available online at http://ieeexplore.ieee.org.

Digital Object Identifier 10.1109/TVT.2017.2711920

However, by reviewing those methods above, we found that they would encounter some issues in massive MIMO system. The complexity of antenna selection will dramatically increase as the number of antennas grows, which makes it impractical for massive MIMO system. Spatial modulation is realized at the cost of capacity loss, which counteracts the benefit brought by massive MIMO. RF chains reduction in mmWave systems, however, still needs many active phase shifters. In addition, these existing methods usually consider linear array, while two-dimensional (2D) array is expected to be implemented in massive MIMO system in order to break the constraint in array aperture as well as resolve signal paths in elevation domain [6]. Some of recent techniques, like continuous aperture phased (CAP) MIMO [18], beamspace MIMO [19], [20] and Electromagnetic (EM) lens enabled MIMO [21], can cope with or extend to 2D apertures, however, the single RF chain has to handle the total power fed to the aperture. Such high power capacity for some expensive RF components like power amplifier is unacceptable.

In this paper, we propose a new technique named vertical spatial filtering (VSF) to reduce the RF complexity in massive MIMO systems for UMa cellular networks. The reduced system with VSF is able to save RF chains in vertical dimension of 2D array while keeps the performance close to the complete system. The concept of VSF, which consists of beam mapping and beam selection, is driven by the following three factors: (i) massive MIMO antennas are expected to be configured in a 2D array structure in BS side; (ii) signals tend to arrive at BS within a restricted range of elevation angles in UMa cellular environments [6], [29]; (iii) beamforming in RF domain can be easily realized with low hardware cost. Factor (i) indicates that beamforming in elevation domain is now considered in massive MIMO systems by using antennas in vertical array dimension. Factor (ii), as it will be shown in this paper, leads to the spatial beam redundancy in vertical array dimension. By further considering factor (iii), we first transform signals from antenna space into beam space (beam mapping) using RF beamforming network implemented in vertical array dimension and then merely select part of vertical beams (beam selection) in elevation domain. It is worth noting that RF beamforming applied in VSF is mainly used for signal coverage [22] other than user communication [23]. Therefore active phase shifters are not necessary and RF beamforming can be simply realized by passive networks. Furthermore, beam selection is regarded as part of cell configuration, which should be done before BS starts to provide services. Neither beam switch network nor instant selection algorithm are needed. Last but not least, although VSF is discussed only in massive MIMO systems for UMa cellular networks in this paper, it can also be applied in other environments or extended to other promising 5G technologies, such as high speed train (HST) systems [24] with distrubuted massive MIMO [25], [26], only if above factors (i) and (ii) still exist.

It is worth noting that as beamforming is carried out only in vertical dimension of the 2D array while horizontal dimension remains unchanged, existing techniques like antenna selection or spatial modulation can be incorporated and implemented in horizontal dimension to further reduce RF complexity. In addition, as will be demonstrated in Section III-A, power capacity of the RF chain will be more acceptable than 2D beamforming techniques [27], [28].

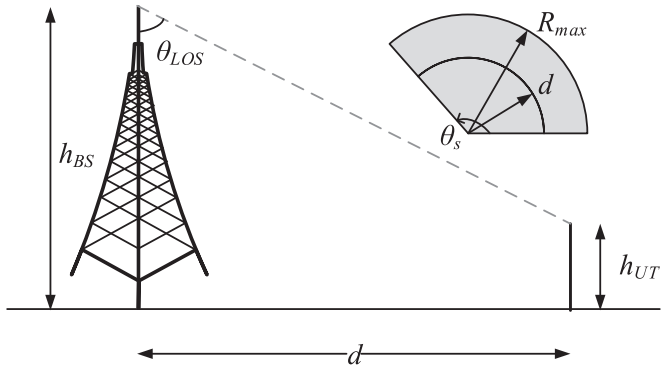


Fig. 1. Simplified BS and MS scenario.

The rest of the paper is organized as follows. Section II introduces the spatial beam redundancy in elevation domain together with a three-dimensional (3D) channel model defined by the 3rd Generation Partnership Project (3GPP), which could deal with channel properties in both elevation and azimuth domains. Section III is focused on VSF, describing beam mapping and beam selection and proposing two strategies for beam selection. Section IV describes the system model with VSF. Numerical results are presented in Section V, and finally conclusions are drawn in Section VI.

*Notation*: Lower case boldfaced letters denote vectors while upper case boldfaced letters denote matrices; $tr(\cdot)$ denotes the trace of a matrix; $(\cdot)^H$, $(\cdot)^T$, $(\cdot)^*$ and $(\cdot)^{-1}$ are used respectively for Hermitian transpose, transpose, complex conjugate and inversion; $[\cdot]_{k,l}$ denotes the matrix element in $k$th row and $l$th column; $\mathbf{I}_N$ is the $N \times N$ identity matrix; $\mathbf{0}_{M\times N}$ is the $M \times N$ all-zeros matrix; Expectation is denoted by $\mathbb{E}(\cdot)$.

## II. Spatial Beam Redundancy

### A. Consideration in Elevation Domain

In UMa scenarios, BS is above all surrounding buildings. Intuitively, signals transmitted by UTs (User Terminal) or scattered by surrounding objects are in the lower half space from the view of BS array. Therefore, there is no need for BS to generate beams towards upper half space where no desired signals exist, which implies that there exists spatial beam redundancy in practical systems.

To further study the spatial beam redundancy mathematically, we first consider a simplified scenario as shown in Fig. 1, where $h_{BS}$ and $h_{UT}$ denote the height of BS and UT , respectively, $d$ is the horizontal distance between BS and UT, $\theta_{LOS}$ is the elevation angle of line-of-sight (LOS) signal, $R_{\max}$ is the cell radius, and $\theta_s$ is the angle of sector coverage. Supposing the uniform distribution of UTs' positions in a sector, the number of UTs with the same $d$ is proportional to the arc length $d \cdot \theta_s$, leading to $d$ following the triangular distribution [36] with the probability density function ($pdf$) as

$$pdf\ (d) = \frac{2d}{R_{\max}^2}. \tag{1}$$

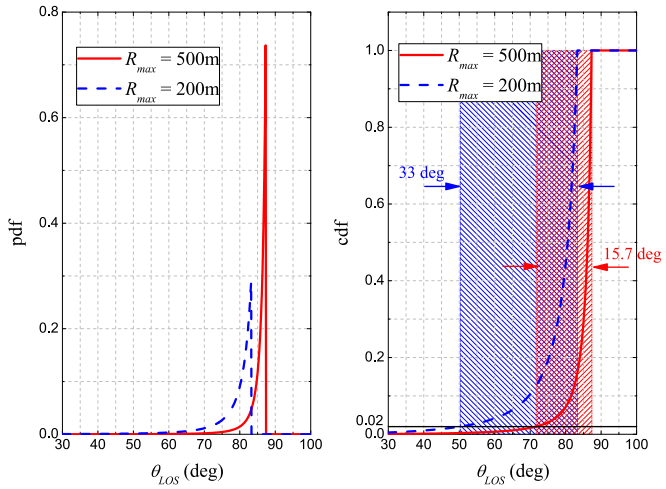


Fig. 2. Probability density function (left) and cumulative distribution function (right) for $\theta_{LOS}$. The shadow area indicates the angle range of 98% coverage.

Considering the relationship between $d$ and $\theta_{LOS}$:

$$\theta_{LOS} = \arctan \frac{d}{h_{BS} - h_{UT}}, \tag{2}$$

the $pdf$ and cumulative distribution function ($cdf$) of $\theta_{LOS}$ can be derived as

$$pdf\left(\theta_{LOS}\right) = \frac{2(h_{BS} - h_{UT})^2 \tan\theta_{LOS} \sec^2\theta_{LOS}}{R_{\max}^2}, \tag{3}$$

and

$$cdf\left(\theta_{LOS}\right) = \frac{(h_{BS} - h_{UT})^2 \tan^2\theta_{LOS}}{R_{\max}^2}, \tag{4}$$

respectively. Fig. 2 illustrates these two functions with $h_{BS} = 25$ m, $h_{UT} = 1.5$ m, where two different cases of cell radius, $R_{\max} = 200$ m and $R_{\max} = 500$ m. It is clear that $\theta_{LOS}$ is mainly concentrated upon small ranges and will get even more concentrated when cell radius is larger. As can be derived from Fig. 2, the minimum angular range is only 33° and 15.7° for 98 percentage coverage for $R_{\max} = 200$ m and 500 m, respectively. If we define the redundancy rate $R$ as

$$R = 1 - \frac{\theta_d}{\Theta}, \tag{5}$$

where $\theta_d$ is the desired angular range, and $\Theta = 180°$ is coverage ability of a BS array in elevation domain. Then, the redundancy rate $R$ of each case is calculated to be 81.7% and 91.3%, respectively. This indicates that large spatial beam redundancy still exists in the lower half space due to the user distribution.

### B. 3D Channel Model

Common 2D channel model [35] only describes channel properties in azimuth domain, which is not suitable for our study as channel properties in elevation domain should also be considered in this paper. Therefore, we adopt a reliable 3D channel model newly defined by 3GPP [36]. The main feature of this model is the introduction of parameters in elevation domain, e.g., angle of arrival, angle of departure and angle spread.

Similar with 2D channel model, the channel coefficient of 3D channel is also assumed to be the sum of contributions of several ($L$) scattering clusters, each of which has several ($S$) rays. The difference is that each ray is defined by parameters both in azimuth and elevation domain. For example, the angle of arrival is defined by single parameter $\phi$ in 2D channel model while it is defined by two parameters $(\theta, \phi)$ in 3D channel model. For convenience, we assume that the field pattern of the element antennas are isotropic and only single linear polarization is considered. Therefore, the channel coefficient between the $k$th UT and the element antenna in the $m$th row and the $n$th column of the BS array can be expressed as [36]

$$[\mathbf{H}]_{m+(n-1)\times M,k} = \sum_{l=1}^{L}\sum_{s=1}^{S} \sqrt{P_l/S}\exp\left(j\Phi_{ls}\right)\cdot \exp\left(j2\pi\lambda^{-1}\left(\hat{\mathbf{r}}_{ls,BS}^{T}\mathbf{d}_{mn,BS}\right)\right) \tag{6}$$

where $P_l$ is the power of the $l$th cluster, $\Phi_{ls}$ is an random initial phase for the $s$th ray in the $l$th cluster, $\hat{\mathbf{r}}_{ls,BS}$ is the spherical unit vector of BS array given by

$$\hat{\mathbf{r}}_{ls,BS} = \begin{bmatrix} \sin\theta_{ls,ZOA}\cos\phi_{ls,AOA} \\ \sin\theta_{ls,ZOA}\sin\phi_{ls,AOA} \\ \cos\theta_{ls,ZOA} \end{bmatrix}, \tag{7}$$

where $\phi_{ls,AOA}$ ($\theta_{ls,ZOA}$) is the azimuth (elevation) angle of arrival at BS, $\mathbf{d}_{mn,BT}$ is the location vector of BS element antenna in the $m$th row and the $n$th column, $\lambda$ is the wavelength of carrier frequency.

As defined in [36], the angle of a certain non-line-of-sight (NLOS) cluster with respect to LOS angle is associated with the power of this cluster. Statistically, the angle would be smaller if the power is stronger. That is to say, clusters with higher power are closer to LOS direction. This assumption is reasonable in real physical environments as clusters far away from the LOS direction usually experience more path loss due to longer path distance or multiple scatters.

Fig. 3 shows the power angular spectrum (PAS) within a 120° sector derived from 3GPP 3D channel model. In order to fully demonstrate the statistic property, we add up the power of signals from 10000 UTs. Considering the case that there are 12 clusters for each UT and 20 rays for each cluster, the total number of rays is up to 2.4 million. It is clear that vast majority of signal power is constrained in a small area in elevation domain, which is consistent with the result in Fig. 2. However, difference should be noted between these two results. Fig. 3 is the case of NLOS environment, while Fig. 2 can be approximately regarded as an LOS case where the Ricean K-factor tends to infinity and signals from different directions have the same power. Result shown in Fig. 3 is important for the proposed VSF technique as it guarantees the prerequisite of spatial beam redundancy even in NLOS environment.

Measured results of channel properties also can be found in [29], where a field measurement campaign is carried out for characterizing the 3D MIMO channel, particularly in elevation

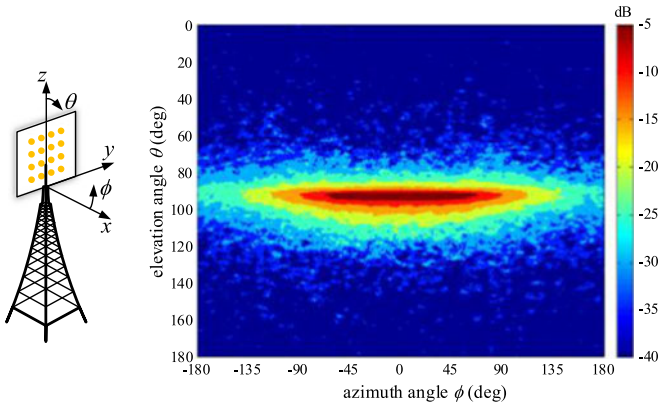


Fig. 3. Simulated power angular spectrum at BS array in NLOS environment with 10000 UTs. Sector angle is 120° in azimuth domain. The result is normalized by maximum value.

domain, in a typical macro urban area (UMa) environment in Beijing, which verified the results discussed above.

Therefore, if we could find a way to discard these redundant beams and preserve those desired beams in elevation domain, large amount of RF chains might be saved while system performance could still be maintained. VSF is such a way to achieve this goal.

## III. Vertical Spatial Filtering (VSF)

### A. Overview

Fig. 4 shows the block diagram of the reduced system with VSF. Suppose that the 2D BS array is deployed in a rectangular configuration with $M$ element antennas in vertical dimension (columns) and $N$ element antennas in horizontal dimension (rows). Conventionally, the number of RF chains should be the same as the total number of element antennas, i.e., $M \times N$. However, with VSF implemented between 2D array and RF front end, the number of RF chains can be reduced to $L \times N$. The principle is described as follows. $N$ identical beam mapping networks are first implemented behind each column of the 2D array, which is responsible for transforming the received signals from antenna space (constructed by output of $M$ antenna ports) into beam space (constructed by output of $M$ beam ports). Thanks to the spatial beam redundancy in elevation domain, some of the beam ports have negligible signal output, therefore only $L$ rows of them ($L < M$) are required to connect to subsequent RF chains while the remained $M - L$ rows of beam ports can be discarded (terminated with impedance matching components). According to the above description, we could divide VSF into two parts, beam mapping and beam selection, all in vertical array dimension as indicated in Fig. 4.

Before we elaborate these two parts, one important fact is worth being stressed. Compared with antenna selection [8]–[10], there is neither switch network nor instant selection algorithm in the proposed scheme when BS is communicating with UTs. This is because that beam selection depends not on a specific UT position but on the statical property of the UT distribution. That is to say, beam selection is done at the stage of cell configuration and those $L$ out of $M$ rows of beam ports are the same for all UTs. Furthermore, Fig. 5 shows the comparison between the vertical beam mapping and 2D beamforming technology [27], [28]. From theoretical discussion, they are the same as they are all based on butler network. However there are still two major differences. One is the RF cost and the other is system robust. First we take an example to discuss RF cost. Assuming that the array size is $10 \times 10$ and each antenna element carries the power of 0.1 W. For 2D beamforming, as a single RF chain has to illuminate all the antennas, power capacity of the power amplifier (PA) in this RF chain should be larger than 10 W ($10 \times 10 \times 0.1$). While for the proposed scheme, a single RF chain should only support a column (10), power capacity of its PA should only larger than 1 W ($10 \times 0.1$). As the cost of PA increases dramatically with the power capacity, vertical beamforming outperforms 2D beamforming in terms of RF cost. Then we consider system robust. As a specific area is covered by only one single beam for 2D beamforming, when this beam is failure, this area is beyond the coverage, which is totally unacceptable from the respect of user experience. While for vertical beam mapping, as any area is covered by several beams, the impact of single beam failure is minor.

As VSF is implemented in vertical dimension and all the columns of BS array have the same operation, the following discussion will first focus on a single column, i.e., an $M$-element linear array. And then give the system model with 2D array in Section IV.

### B. Beam Mapping

Beam mapping is a transformation from antenna space to beam space. Several methods can be used to realize the mapping matrix, like Butler network [32] or transmit arrays [33]. The following discussion will be based on Butler network. Referring to microwave network theory, beam mapping can be described as

$$\mathbf{b} = \mathbf{T}\mathbf{s}, \tag{8}$$

where $\mathbf{s}$ and $\mathbf{b}$ are both $M \times 1$ vectors representing received signals on a single column of BS array in antenna space and beam space, respectively. $\mathbf{T}$ is an $M \times M$ **mapping matrix** composed of scattering parameters from antenna ports to beam ports. As the beam mapping network is considered to be passive and lossless, $\mathbf{T}$ should satisfy the condition of unitary matrix, i.e.,

$$\mathbf{T}^H\mathbf{T} = \mathbf{T}\mathbf{T}^H = \mathbf{I}, \tag{9}$$

which is able to preserve the signal power in both antenna space and beam space. The following discussion shows the derivation of $\mathbf{T}$.

As known from antenna array theory [30], when a complete description of the desired antenna pattern is given, the antenna excitations in a uniform linear array (ULA) can be determined by beamforming technology. The antenna pattern $f_d(\theta)$ described by these antenna excitations is

$$f_d(\theta) = \sum_{m=1}^{M} \alpha_m c_m(\theta), \tag{10}$$

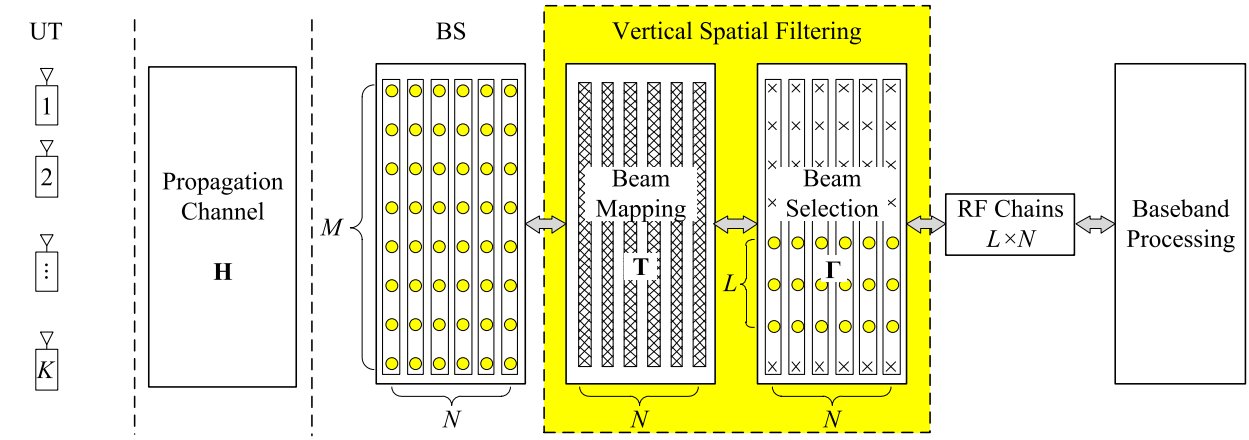


Fig. 4. Block diagram of the reduced system with VSF: UTs are all equipped with a single antenna; BS is equipped with a 2D antenna array that has $M$ rows and $N$ columns; $N$ identical beam mapping networks are implemented behind each column of the 2D array; $L$ out of $M$ rows of beam ports are selected for further baseband processing.

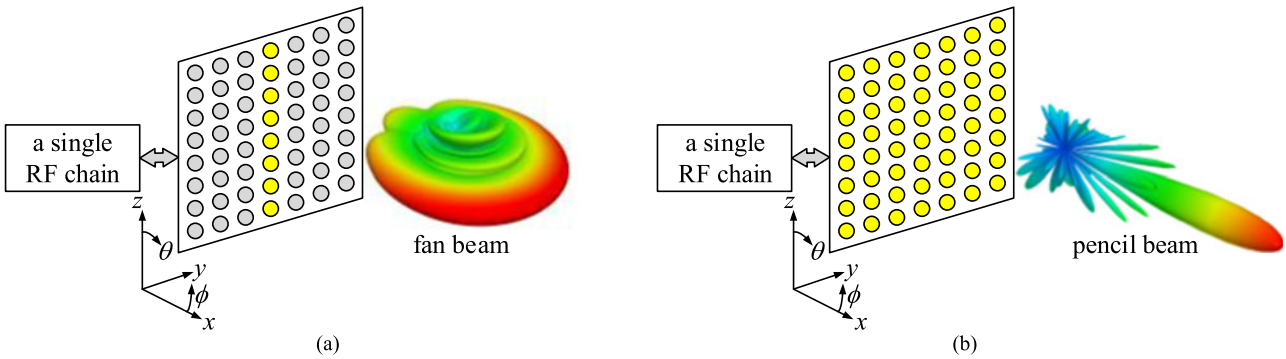


Fig. 5. Comparison between vertical beam mapping and 2D beamforming fed by a single RF chain. (a) vertical beam mapping: only a column of elements are illuminated. (b) 2D beamforming: all the elements are illuminated.

where $\theta$ is the angle of observation direction relative to the axis of the ULA, $M$ is the total number of antennas, $\alpha_m$ is the excitation of the $m$th antenna, and $c_m(\theta)$ is array steering weight for the $m$th antenna which is expressed as

$$c_m(\theta) = \exp\left(j\frac{2\pi}{\lambda}(M-m)d\cos\theta\right), \tag{11}$$

where $\lambda$ is the wavelength of carrier frequency, $d$ is the element space for ULA. Thus, $M$ independent basis patterns (or beams) $f_k(\theta)$ (for $k = 1, 2, \cdots, M$), whose main lobes point to $M$ different directions $\theta_k$, can be derived as

$$f_k(\theta) = \sum_{m=1}^{M} \alpha_{m,k} c_m(\theta), \tag{12}$$

where

$$\alpha_{m,k} = |\alpha_{m,k}| \exp\left(-j\frac{2\pi}{\lambda}(M-m)d\cos\theta_k\right). \tag{13}$$

Equations (11), (12) and (13) indicate that signals transmitted by $M$ antennas sum in phase at the direction of angle $\theta_k$ for basis pattern $f_k(\theta)$, thus making the main lobe of $f_k(\theta)$ points to $\theta_k$.

As the degrees of freedom for antenna space and beam space are the same (both of them are $M$), any desired antenna pattern synthesized by array antennas can be definitely synthesized by these basis beams, i.e.,

$$f_d(\theta) = \sum_{k=1}^{M} \beta_k f_k(\theta) = \sum_{k=1}^{M}\sum_{m=1}^{M} \alpha_{m,k}\beta_k c_m(\theta), \tag{14}$$

where $\beta_k$ is the weight of the $k$th basis beam. From (10) and (14), we can derive the transformation from beam weights to antenna excitations,

$$[\alpha_1, \alpha_2, \cdots, \alpha_m]^T = \mathbf{T}_b \cdot [\beta_1, \beta_2, \cdots, \beta_m]^T, \tag{15}$$

where

$$\mathbf{T}_b = \begin{bmatrix} \alpha_{1,1} & \alpha_{1,2} & \cdots & \alpha_{1,M} \\ \alpha_{2,1} & \alpha_{2,2} & \cdots & \alpha_{2,M} \\ \vdots & \vdots & \ddots & \vdots \\ \alpha_{M,1} & \alpha_{M,2} & \cdots & \alpha_{M,M} \end{bmatrix}. \tag{16}$$

The relationship between $\mathbf{T}_b$ and the mapping matrix $\mathbf{T}$ in (8) is

$$\mathbf{T} = \mathbf{T}_b^T, \tag{17}$$

which is due to the reciprocity of passive network. Because $[\mathbf{T}_b]_{m,k}$ is the scattering parameter from beam ports $\#k$ to an-

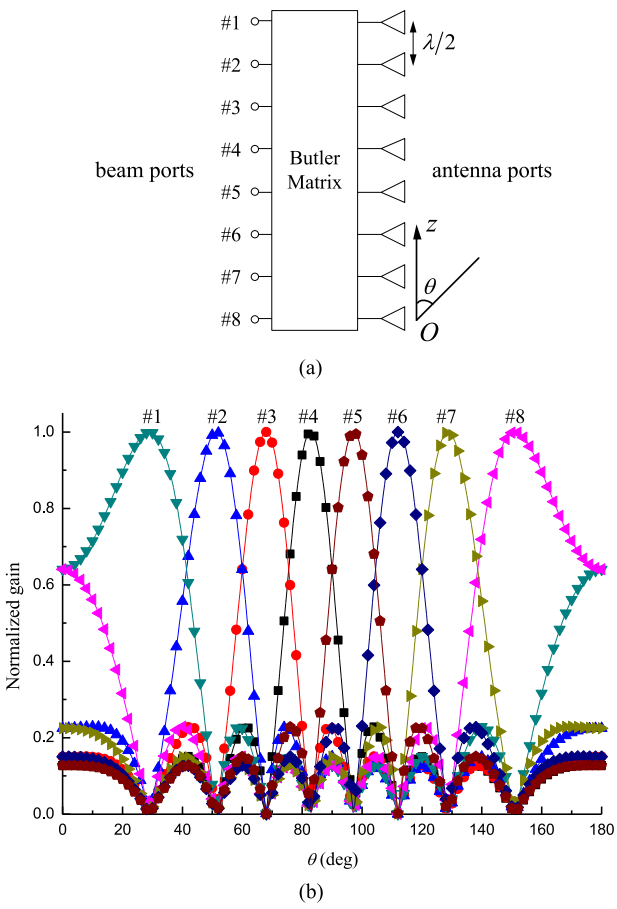


Fig. 6. Basis patterns for 8-vertical-element ULA: (a) Block diagram of $8 \times 8$ mapping network; (b) Mapping beams corresponding to input ports.

tenna port $\#m$, while $[\mathbf{T}]_{k,m}$ is the scattering parameter from antenna port $\#m$ to beam port $\#k$. These two scattering parameters should be the same for a pass microwave network [31]. It is obvious that (8) is related to receiving mode (uplink) while (15) is related to transmitting mode (downlink).

As an example, Fig. 6 shows the case of Butler network with an 8-vertical-element $\lambda/2$-spaced ULA whose antennas have isotropic radiation patterns. The circuit diagram of an $8 \times 8$ Butler network can be found in [34]. We only give the expression of the mapping matrix $\mathbf{T}$ used in this paper. For each beam port, the Butler network generates progressive phase shifts (PPS) at the antenna ports with equal amplitude. For an $M \times M$ Butler network, there are $M$ PPS and the PPS for the $k$th beam port satisfies

$$\frac{M+1-2k}{M}\pi = \frac{2\pi}{\lambda} d \cos\theta_k. \tag{18}$$

Substituting (18) into (13), we can derive the antenna excitations for $k$th basis beam as

$$\alpha_{m,k} = \frac{1}{\sqrt{M}} \exp\left(-j\frac{\pi}{M}(M+1-2k)(M-m)\right). \tag{19}$$

Basis patterns shown in Fig. 6(b) can be obtained by substituting (11) and (19) into (12). Finally, the mapping matrix $\mathbf{T}$ is derived by (16), (17), and (19), which is expressed as

$$[\mathbf{T}]_{m,k} = \frac{1}{\sqrt{M}} \exp\left(-j\frac{\pi}{M}(M+1-2m)(M-k)\right). \tag{20}$$

It is obvious from Fig. 6 that the maximum direction of one pattern is at nulls of all others. This is due to the orthogonal nature of these patterns derived by Butler matrix. These patterns together cover the whole elevation space (from 0° to 180°), thus some input ports whose output patterns point to undesired space can be discarded. Nevertheless, desired user signals or multipath information can still be preserved and only a small amount of beamforming gain might be lost.

### C. Beam Selection

Beam selection, which selects $L$ out of $M$ beams after the operation of beam mapping, can be expressed by using an $L \times M$ row-selecting matrix $\mathbf{\Lambda}$ as

$$\widetilde{\mathbf{b}} = \mathbf{\Lambda}\mathbf{b}, \tag{21}$$

where $\widetilde{\mathbf{b}}$ is an $L \times 1$ vector denoting signals on $L$ selected beams. Suppose these $L$ selected beams are predefined in a vector

$$\mathbf{p} = [p_1, p_2, \cdots, p_L], \tag{22}$$

where $p_l \in \{1, 2, \cdots, M\}$ (for $l = 1, 2, \cdots, L$) is the beam index. The element of $\mathbf{\Lambda}$ would be

$$[\mathbf{\Lambda}]_{l,m} = \begin{cases} 1, & m = p_l, \\ 0, & m \neq p_l. \end{cases} \tag{23}$$

By substituting (8) into (21), the received signals on a single column of 2D array after VSF can be expressed as

$$\widetilde{\mathbf{b}} = \mathbf{\Lambda}\mathbf{T}\mathbf{s}. \tag{24}$$

The most important thing for VSF is to determine how many beams and which beam set should be used. In general, beam selection mainly depends on two factors. One is the statistical characteristics of PAS as plotted in Fig. 3, and the other is the acceptable system performance loss. The first factor is related to the channel measurement campaign in real scenarios. While the second factor implies a trade-off between system performance and system complexity.

In the following discussion, we define $\eta$ as the signal power ratio for signals restricted in a certain elevation angle range $[\theta_1, \theta_2]$,

$$\eta = \int_{\theta_1}^{\theta_2}\int_0^{2\pi} P(\theta,\phi)\sin\theta \mathrm{d}\theta\mathrm{d}\phi = \int_{\theta_1}^{\theta_2} P_\theta(\theta)\sin\theta\mathrm{d}\theta, \tag{25}$$

where $P(\theta, \phi)$ is the normalized PAS satisfying

$$\int_0^{\pi}\int_0^{2\pi} P(\theta,\phi)\sin\theta\mathrm{d}\theta\mathrm{d}\phi = 1. \tag{26}$$

and

$$P_\theta(\theta) = \int_0^{2\pi} P(\theta,\phi)\mathrm{d}\phi. \tag{27}$$

Now we propose two strategies for beam selection.

*1) Given $\eta$, Minimize the Number of Required Beam:* The required beam set is related to signal coverage, therefore we should first minimize the range of elevation angle where power ratio is no less than the given $\eta$.

This strategy can be obtained by solving the following optimization problem:

$$\begin{aligned} &\min\left(\theta_2-\theta_1\right)\\ &\text{s.t.}\int_{\theta_1}^{\theta_2} P_\theta\left(\theta\right)\sin\theta d\theta\geq\eta\\ &\qquad 0\leq\theta_1<\theta_2\leq\pi \end{aligned} \tag{28}$$

By studying the results in Fig. 3, we can speculate that $P_\theta\left(\theta\right)\sin\theta$ is an unimodal function in $\theta\in[0,\pi]$, which has a single maximum value. We can search $\theta_1$ ($\theta_2$) starting from its peak position $\theta_m$ to its right (left) side. If we use

$$P_\theta\left(\theta_1\right)\sin\theta_1=P_\theta\left(\theta_2\right)\sin\theta_2 \tag{29}$$

as a constraint condition during the searching process, we can guarantee that any values of $P_\theta\left(\theta\right)\sin\theta$ in $[\theta_1,\theta_2]$ is larger than those out of this range. Therefore, when (25) is satisfied, $\theta_2-\theta_1$ must be the minimum for the given $\eta$.

However, PAS is derived by channel measurement in real scenario, where results are all discrete. Therefore discrete version of searching method described above should be used to determine $\theta_1$ and $\theta_2$, which is detailed in Algorithm 1. After that, we can solve the following optimization problem to determine how many beams ($L$) and which beam set ($\mathbf{p}$) should be used:

$$\begin{aligned} &\min L\\ &\text{s.t.}\\ &\{\#p_1,\#p_2,\cdots,\#p_L\}\subset\{\#1,\#2,\cdots,\#M\}\\ &[\theta_1,\theta_2]\subseteq\bigcup_{l=1}^{L}BW_{3dB}^{(\#p_l)},\\ &[\theta_1,\theta_2]\not\subset\bigcup_{l=1}^{L}BW_{3dB}^{(\#p_l)}-BW_{3dB}^{(\#p_s)},\forall s\in[1,2,\cdots,L] \end{aligned} \tag{30}$$

where index $\#p_l$ and $BW_{3dB}^{(\#p_l)}$ denote the $l$th required beam and its 3 dB beamwidth coverage. (30) means that the required beam set $\mathbf{p}=\{\#p_1,\#p_2,\cdots,\#p_L\}$ should be the minimum beam set whose 3dB beamwidth jointly covers elevation angle range $[\theta_1,\theta_2]$.

By using Algorithm 1 we find that 99% of signal power is restricted in the elevation angle between 75° and 121°. Referring to Fig. 6(b), assuming BS array has 8 antennas in vertical dimension, we found that three beams of $\#4(p_1)$, $\#5(p_2)$, and $\#6(p_3)$ are sufficient to cover the range of $[75^\circ,121^\circ]$. Therefore, the row-selecting matrix $\mathbf{\Lambda}$ defined in (21) should be

$$\mathbf{\Lambda}=\begin{bmatrix}0&0&0&1&0&0&0&0\\0&0&0&0&1&0&0&0\\0&0&0&0&0&1&0&0\end{bmatrix}. \tag{31}$$

**Algorithm 1:** Determine signal coverage.

**Input:**
(1) discretized elevation angle set: $\theta^{(n)}$;
(2) PAS corresponding to discretized angles: $P_\theta^{(n)}$;
(3) the given power ratio: $\eta$;

**Output:** $\theta_1,\theta_2$

$m:=\arg\max_n\left(P_\theta^{(n)}\sin\theta^{(n)}\right)$
$n1:=m$
$n2:=m$
$P_t:=\sum_n P_\theta^{(n)}\sin\theta^{(n)}$
**while** $\sum_{n=n1}^{n2}P_\theta^{(n)}\sin\theta^{(n)}\Big/P_t<\eta$ **do**
  $n2:=n2+1$
  **while** $P_\theta^{(n1)}\sin\theta^{(n1)}>P_\theta^{(n2)}\sin\theta^{(n2)}$ **do**
    $n1:=n1-1$
  **end while**
**end while**
$\theta_1=\theta^{(n1)}$
$\theta_2=\theta^{(n2)}$

*2) Given Number of Required Beams, Maximize $\eta$:* If the number of beams ($L$) is pre-decided due to the consideration of system complexity, the selected beams should cover the range where signal power ratio $\eta$ is maximized. The selected beam set $\mathbf{p}$ should satisfy the following condition

$$[\theta_{m1},\theta_{m2}]=\arg\max_{[\theta_1,\theta_2]}\int_{\theta_1}^{\theta_2}P_\theta\left(\theta\right)\sin\theta d\theta, \tag{32}$$

where

$$[\theta_1,\theta_2]=\bigcup_{l=1}^{L}BW_{3dB}^{(\#p_l)}. \tag{33}$$

Similar to Algorithm 1, we can search the required beams from the beam that covers the peak direction, which is described in Algorithm 2. As an example, if only two beams can be used in an array with 8 antennas, beams of #4 and #5 should be selected.

A simple empirical method can be also used to determine the beams for PAS shown in Fig. 3, which is described as bellow

step 1: Given the specified number of vertical beams $m$ due to the acceptable system complexity;
step 2: The number of vertical beams in upper half space is $\lfloor(m-1)/2\rfloor$, and the selected beams should be those which are close to horizontal plane;
step 3: Then the number of vertical beams in lower half space is $m-\lfloor(m-1)/2\rfloor$, and the selected beams should be those which are close to horizontal plane.

This empirical method is based on the fact seen from Fig. 3 that most signals are near the horizontal plane and those from lower half space are a little more than those from lower half space.

It is worth noting again that beam selection can be regarded as part of cell configuration. It should be done before the system

**Algorithm 2:** Determine beam set.

**Input:**

(1) discretized elevation angle set: $\theta^{(n)}$;

(2) PAS corresponding to discretized angles: $P_\theta^{(n)}$;

(3) the required beam number: $L$;

**Output:** $p1, p2$

$m := \arg\max_n \left( P_\theta^{(n)} \sin\theta^{(n)} \right)$

find $p_m$, s.t. $\theta^{(m)} \in BW_{3dB}^{(pm)}$

$p1 := p_m$

$p2 := p_m$

**while** $p2 - p1 + 1 < L$ **do**

  $\eta_1 := \sum_n P_\theta\left(\theta^{(n)}\right) \sin\theta^{(n)}$, where $\theta^{(n)} \in \bigcup_{p=p1-1}^{p2} BW_{3dB}^{(p)}$

  $\eta_2 := \sum_n P_\theta\left(\theta^{(n)}\right) \sin\theta^{(n)}$, where $\theta^{(n)} \in \bigcup_{p=p1}^{p2+1} BW_{3dB}^{(p)}$

  **if** $\eta_1 < \eta_2$ **then**

    $p2 := p2 + 1$

  **else**

    $p1 := p1 - 1$

  **end if**

**end while**

starts to provide services. Therefore, no additional complexity will be introduced when BS begins to communicate with UTs.

## IV. System Model With VSF

As shown in Fig. 4, the received signals without VSF can be expressed as

$$\mathbf{y} = \mathbf{H}\mathbf{x} + \mathbf{n}, \tag{34}$$

where $\mathbf{y}$ is the $MN \times 1$ received vector, $\mathbf{H}$ is the $MN \times K$ channel matrix whose element $[\mathbf{H}]_{m+(n-1)\times M,k}$ (for $m = 1, 2, \cdots, M, n = 1, 2, \cdots, N, k = 1, 2, \cdots, K$) represents the complex channel gain between the $k$th UT and the element antenna in $m$th row and $n$th column of BS array, $\mathbf{x} = [x_1, x_2, \cdots, x_K]^T$ is a $K \times 1$ vector that contains transmitted signal $x_k$ from the $k$th UT, and $\mathbf{n}$ is the i.i.d additive Gaussian noise vector following the distribution $\mathcal{CN}(0, \sigma_n^2)$.

When VSF is implemented in each column of BS array, the original channel matrix $\mathbf{H}$ can be replaced by a virtual channel matrix $\widetilde{\mathbf{H}}$. Referring to (24), the relationship between these two channel matrices can be expressed as

$$\widetilde{\mathbf{H}} = \mathcal{T}\mathbf{H}, \tag{35}$$

where $\mathcal{T}$ is an $LN \times MN$ matrix extended from $\mathbf{\Lambda T}$ in (24) as

$$\mathcal{T} = \begin{bmatrix} \mathbf{\Lambda T} & \mathbf{0}_{L\times M} & \cdots & \mathbf{0}_{L\times M} \\ \mathbf{0}_{L\times M} & \mathbf{\Lambda T} & \cdots & \mathbf{0}_{L\times M} \\ \vdots & \vdots & \ddots & \vdots \\ \mathbf{0}_{L\times M} & \mathbf{0}_{L\times M} & \cdots & \mathbf{\Lambda T} \end{bmatrix}. \tag{36}$$

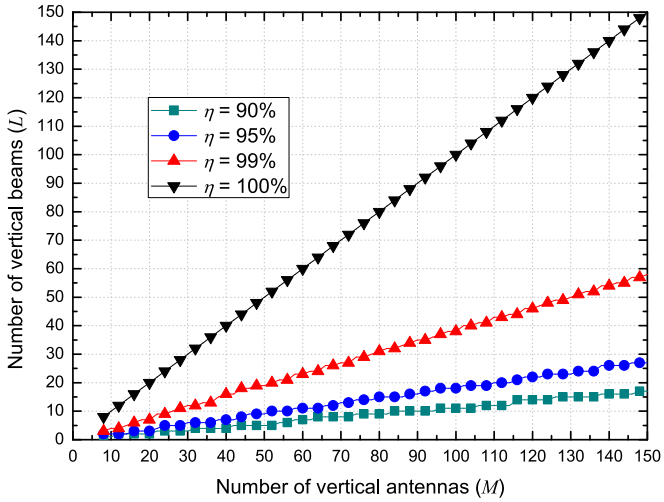


Fig. 7. The number of required beams ($L$) as a function of the number of vertical antennas ($M$), where different $\eta$'s are considered.

Note that $\mathcal{T}$ is expressed in the form of $N \times N$ block matrix, where all diagonal element matrices are $\mathbf{\Lambda T}$ and all non-diagonal element matrices are all-zeros matrix.

Finally, the system model of the reduced system with VSF can be expressed as

$$\widetilde{\mathbf{y}} = \widetilde{\mathbf{H}}\mathbf{x} + \widetilde{\mathbf{n}}, \tag{37}$$

where $\widetilde{\mathbf{y}} = \mathcal{T}\mathbf{y}$, an $LN \times 1$ vector, is the transformed signals in beam space. Similarly, we have $\widetilde{\mathbf{n}} = \mathcal{T}\mathbf{n}$, an $LN \times 1$ vector of i.i.d Gaussian noise variables.

## V. Numerical Results and Discussion

### A. Study of Required beams

Fig. 7 shows the number of required beams ($L$) as a function of the number of vertical antennas ($M$) when different $\eta$'s are considered. The result is derived from Algorithm 1. It is easy to see that less than half of the total vertical beams are needed to achieve a $\eta = 99\%$ signal power coverage. If we lower $\eta$ a little bit, e.g. $\eta = 95\%$, another half of the vertical beams can be discarded further. One more thing we can learn from Fig. 7 is that $L$ increases linearly with $M$ for a given $\eta$, which means the required beam ratio ($L/M$) is corresponding to the given $\eta$. This relationship between $L/M$ and $\eta$ can be derived by using Algorithm 2, and the corresponding result is shown in Fig. 8. We have $L/M = 0.1$ for $\eta = 90\%$, $L/M = 0.17$ for $\eta = 95\%$, and $L/M = 0.38$ for $\eta = 99\%$ from Fig. 8, which indicates significant reduction of RF chains achieved by VSF. When the number of required vertical beams $L$ is small (compared to $M$), adding one more beam could bring huge increase of the signal power coverage while the contribution of adding more beams will not be attractive when $L$ is large.

### B. Single-User System Performance

We first study the performance of the reduced system with VSF for a single user, i.e. $K = 1$. The channel capacity for

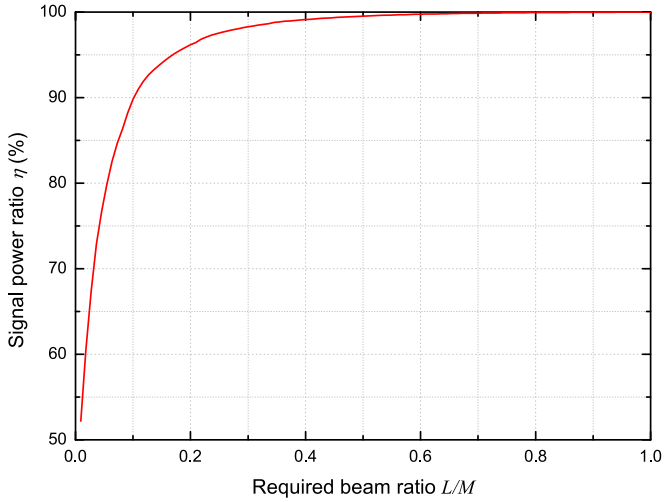


Fig. 8. The signal power ratio $\eta$ as a function of the required beam ratio $(L/M)$.

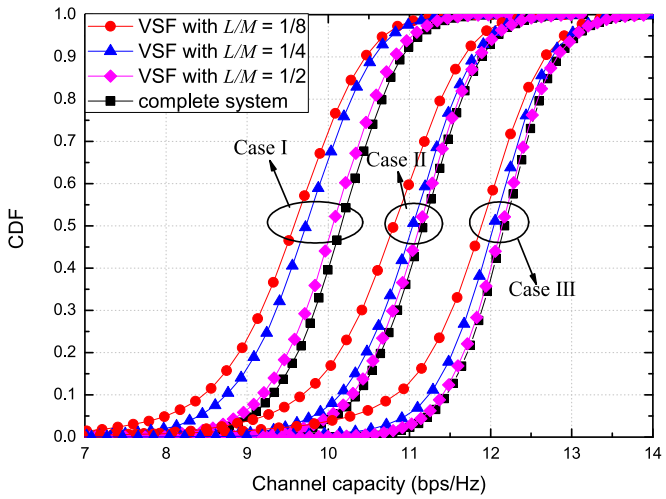


Fig. 9. CDF of the channel capacity for single-user system in three cases; Case I: $M = 8, N = 16$; Case II: $M = 16, N = 16$; Case III: $M = 32, N = 16$.

conventional complete system $C_0$ is well known to be

$$C_0 = \log_2\left(1 + \rho \mathbf{H}^H \mathbf{H}\right), \tag{38}$$

where $\mathbf{H}$ is defined in (34), $\rho = P/\sigma_n^2$ is the nominal SNR. As for the reduced system with VSF, the channel capacity $C_{VSF}$ is given by

$$C_{VSF} = \log_2\left(1 + \rho \widetilde{\mathbf{H}}^H \widetilde{\mathbf{H}}\right), \tag{39}$$

where $\widetilde{\mathbf{H}}$ is defined in (35). In this section, we use Butler network (20) to realize beam mapping.

Fig. 9 shows the CDF of channel capacity when three different cases of BS configurations are considered with SNR = 10 dB, where the number of horizontal antennas is fixed as $N = 16$ but number of vertical antennas are $M = 8$, $M = 16$, and $M = 32$, respectively. In each case, three required beam ratios $L/M$ are compared. Therefore, the second strategy for the beam selection is applied. For simplicity, empirical method is used to select beams for specified beam numbers. It is clear from Fig. 9 that with the increased $L/M$ in each case, CDF curve of the reduced system with VSF gets closer to the result of the complete system. By Comparing case I and case II (or case II and case III), we can find that performance of case II with half of vertical beams is much better than that of case I with full system while the number of vertical beams $L$ are the same in both cases. The above example shows that with the same RF complexity, reduced system with VSF outperforms the complete system. This is caused by the fact that higher channel gain can be achieved by larger $M$, which also leads to the result that the performance in case II with only two vertical beams $(L/M = 1/8)$ is still better than that in case I with eight vertical beams (complete system).

TABLE I
RELATIVE PERCENTAGE OF ERGODIC OUTAGE CHANNEL CAPACITY

| L/M | Case I (M = 8) $C_0$ : 10.17 bps/Hz | Case II (M = 16) $C_0$ : 11.18 bps/Hz | Case III (M = 32) $C_0$ : 12.17 bps/Hz |
|---|---|---|---|
| 1/8 | 94.40% | 96.60% | 97.62% |
| 1/4 | 95.77% | 98.84% | 98.93% |
| 1/2 | 99.12% | 99.46% | 99.67% |

Table I lists the ergodic outage channel capacity derived from Fig. 9 for three different cases. The first row shows the absolute values $C_0$ of the complete systems while for the reduced system with VSF, results are given by relative percentage normalized by $C_0$. We find that the percentage increases not only with higher $L/M$ but also with larger $M$, which indicates that when $L/M$ is fixed, the performance of the reduced system with VSF is closer to its full system if the array becomes larger. This is duo to the higher beam resolution in elevation domain, which enhances with the increased number of vertical antennas, thus making it easier for the system to direct the main lobe to the UT. However, higher beam resolution also means more RF chains even when the RF-complexity of the system is reduced. Therefore, we should jointly consider the system performance, BS array scale and the redundancy rate, indicating trade-offs between these three factors.

### C. Multi-User System Performance

Now we consider the performance in multi-user scenarios. Different from FFT-based antenna selection [9], the reduced system with VSF does not require selection algorithm as the reduced RF-chains are determined by the system configuration. Therefore, it will be more efficient in multi-user systems. We study the sum-rate capacity and BER performance in multi-user MIMO systems in this part.

Let $\mathbf{h}_k \in \mathbb{C}^{MN\times 1}$ denote the $k$th column of $\mathbf{H}$, representing the channel coefficient vector between the $k$th UT and BS. We use MMSE [37], [38] to maximize the post-detection signal-to-interference plus noise ratio (SINR) for each UT. The received interference-plus-noise correlation matrix $\mathbf{R}_{nn,k}$ for the $k$th UT

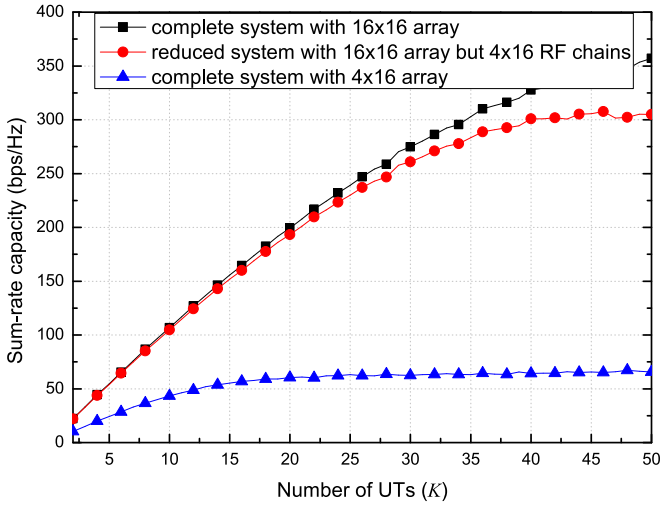


Fig. 10. Sum-rate capacity comparison between the reduced system with VSF and two complete systems.

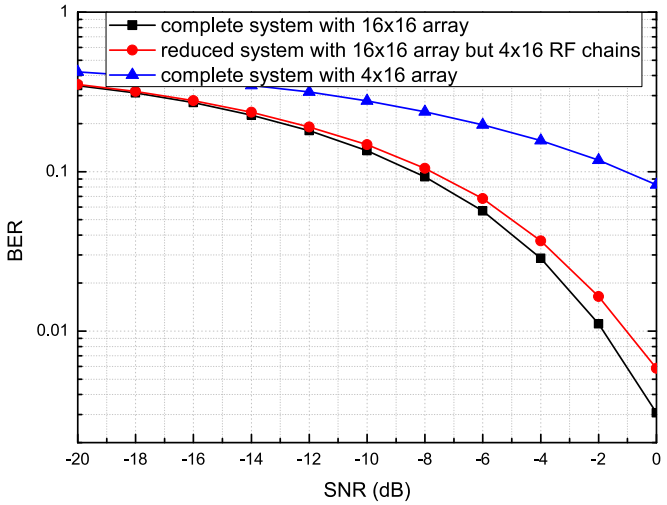


Fig. 11. BER performance comparison between the reduced system with VSF and two complete systems, where $K = 10$.

is given by

$$\mathbf{R}_{nn,k} = \sigma_n^2 \mathbf{I}_{MN} + \sum_{j=1, j\neq k}^{K} \mathbf{h}_j^* \mathbf{h}_j^T, \tag{40}$$

and the correspongding weight $\mathbf{w}_k$ that maximizes the output SINR is

$$\mathbf{w}_k = \mathbf{R}_{nn,k}^{-1} \mathbf{h}_k^*. \tag{41}$$

Then, we can derive the expression of SINR for the $k$th UT as

$$SINR_k = \frac{\mathbf{w}_k^H \mathbf{h}_k^* \mathbf{h}_u^T \mathbf{w}_k}{\mathbf{w}_k^H \mathbf{R}_{nn,k} \mathbf{w}_k} \tag{42}$$

and thus the sum-rate capacity is

$$C_{\text{sum}} = \mathbb{E}\left\{ \sum_{k=1}^{K} \log_2 \left(1 + SINR_k\right) \right\}. \tag{43}$$

The expression for the reduced system with VSF can be obtained in the same way.

Three systems are compared in this section: complete system with $16 \times 16$ array, reduced system with $16 \times 16$ array but $4 \times 16$ RF chains, and complete system with $4 \times 16$ array. Fig. 10 shows the sum-rate capacity against the number of UTs ($K$). We can observe that the sum-rate capacity gap between the reduced system and the complete system with the same array scale is negligible when $K$ is small (e.g., $K \leq 25$ in Fig. 10). However, this gap can be bridged when beam resolution is high enough. When $K$ increases, the sum-rate capacity of the reduced system becomes saturated first, which means less UTs can be supported compared to the complete system. In addition, it is shown that the reduced system outperforms the complete system with the same RF complexity, which again validates the advantage of VSF.

Fig. 11 shows the BER performance comparison between those three considered systems in downlink. Precoding technique of regularized channel inversion [39] is applied to cancel the interference from other UTs, which can be expressed as

$$\mathbf{W} = \beta \mathbf{H}^* \left( \mathbf{H}^T \mathbf{H}^* + \sigma_n^2 \mathbf{I}_K \right)^{-1}, \tag{44}$$

where $\beta$ is a constant factor to maintain the total transmit power and it is given by

$$\beta = \sqrt{\frac{MN}{tr\left(\mathbf{W}\mathbf{W}^H\right)}}. \tag{45}$$

The received signal must be divided by $\beta$ at each UT to compensate for the effect of amplification by this factor. We simulate ten UTs simultaneously to avoid the UT saturation, and keep the same transmit power for all three considered systems. It can be seen from Fig. 11 that the BER performance of the reduced system with VSF is much closer to that of the complete system with the same array scale and outperforms the complete system with the same RF complexity.

## VI. Conclusion

In this paper, a new technique called vertical spatial filtering (VSF) was proposed to reduce the RF complexity in vertical dimension of a massive MIMO planar array for UMa cellular networks. We first introduced the spatial beam redundancy together with a 3D channel model defined by 3GPP. Then, we elaborated VSF by discussing beam mapping and beam selection. Finally, system model with VSF and numerical results are presented to evaluate the system performance. Particularly, VSF is implemented in vertical dimension of BS array and is very attractive for saving RF chains in elevation domain in UMa cellular networks. Considerable RF chains in vertical dimension can be saved due to the high spatial beam redundancy, while very close performance compared to the conventional complete system can be maintained.

## REFERENCES


[1] D. Gesbert, M. Shafi, D. Shiu, P. J. Smith and A. Naguib, "From theory to practice: An overview of MIMO space-time coded wireless systems," *IEEE J. Sel. Areas Commun.*, vol. 21, no. 3, pp. 281–302, Apr. 2003.

[2] "*E-UTRA; LTE Physical Layer-General Description*, R8," 3GPP TS 36.201, 2007.

[3] "*Part 16: Air Interface for Fixed and Mobile Broadband Wireless Access Systems*," IEEE Standard 802.16e_-2005. IEEE Standard 802.16_-2004/Corl-2005, 2006.

[4] J. G. Andrews *et al.*, "What will 5G be?," *IEEE J. Sel. Areas Commun.*, vol. 32, no. 6, pp. 1065–1082, Jun. 2014.

[5] C.-X. Wang *et al.*, "Cellular architecture and key technologies for 5G wireless communication networks," *IEEE Commun. Mag.*, vol. 52, no. 2, pp. 122–130, Feb. 2014.

[6] F. Rusek *et al.*, "Scaling up MIMO: Opportunities and challenges with very large arrays," *IEEE Signal Process. Mag.*, vol. 30, no. 1, pp. 40–46, Jan. 2013.

[7] E. G. Larsson, O. Edfors, F. Tufvesson, and T. L. Marzetta, "Massive MIMO for next generation wireless systems," *IEEE Commun. Mag.*, vol. 52, no. 2, pp. 186–195, Feb. 2014.

[8] A. F. Molisch, M. Z. Win, and J. H. Winters, "Reduced-complexity transmit/receive-diversity systems," *IEEE Trans. Signal Process.*, vol. 51, no. 11, pp. 2729–2738, Nov. 2003.

[9] A. F. Molisch and X. Zhang, "FFT-based hybrid antenna selection schemes for spatially correlated MIMO channels," *IEEE Commun. Lett.*, vol. 8, no. 1, pp. 36–38, Jan. 2004.

[10] X. Zhang, Z. Lv, and W. Wang, "Performance analysis of multiuser diversity in MIMO systems with antenna selection," *IEEE Trans. Wireless Commun.*, vol. 7, no. 1, pp. 15–21, Jan. 2008.

[11] R. Y. Mesleh, H. Haas, S. Sinanovic, C. W. Ahn, and S. Yun, "Spatial modulation," *IEEE Trans. Veh. Technol.*, vol. 57, no. 4, pp. 2228–2241, Jul. 2008.

[12] M. D. Renzo, H. Haas, and P. M. Grant, "Spatial modulation for multiple-antenna wireless systems: A survey," *IEEE Commun. Mag.*, vol. 49, no. 12, pp. 182–191, Dec. 2011.

[13] N. Serafimovski *et al.*, "Practical implementation of spatial modulation," *IEEE Trans. Veh. Technol.*, vol. 62, no. 9, pp. 4511–4523, Nov. 2013.

[14] M. D. Renzo, H. Haas, A. Ghrayeb, and L. Henzo, "Spatial Modulation for generalized MIMO: Challenges, opportunities, and implementation," *Proc. IEEE*, vol. 102, no. 1, pp. 56–103, Jan. 2014.

[15] P. Yang, M. D. Renzo, Y. Xiao, S. Li, and L. Henzo, "Design guidelines for spatial modulation," *IEEE Commun. Surveys Tut.*, vol. 17, no. 1, pp. 6–26, Jan.–Mar. 2015.

[16] P. Yang *et al.*, "Single-carrier SM-MIMO: A promising design for broadband large-scale antenna systems," *IEEE Commun. Surveys Tuts.*, vol. 18, no. 3, pp. 1687–1716, Jul.–Sep. 2016.

[17] O. E. Ayach, S. Rajagopal, S. Abu-Surra, Z. Pi, and R. W. Heath, "Spatially sparse precoding in millimeter wave MIMO systems," *IEEE Trans. Wireless Commun.*, vol. 13, no. 3, pp. 1499–1513, Mar. 2014.

[18] A. Sayeed and N. Behdad, "Continuous aperture phased MIMO: Basic theory and applications," in *Proc. 48th Annu. Allerton Conf. Commun., Control, Comput.*, Sep. 29–Oct. 1, 2010, pp. 1196–1203.

[19] J. Brady, N. Behdad. and A. M. Sayeed, "Beamspace MIMO for millimeter-wave communications: System architecture, modeling, analysis, and measurements," *IEEE Trans. Antennas Propag.*, vol. 61, no. 7, pp. 3814–3827, Jul. 2013.

[20] P. V. Amadori and C. Masouros, "Low RF-complexity millimeter-wave beamspace-MIMO systems by beam selection," *IEEE Trans. Commun.*, vol. 63, no. 6, pp. 2212–2223, Jun. 2015.

[21] Y. Zeng, R. Zhang, and Z. N. Chen, "Electromagnetic lens-focusing antenna enabled massive MIMO: Performance improvement and cost reduction," *IEEE J. Sel. Areas Commun.*, vol. 32, no. 6, pp. 1194–1260, Jun. 2014.

[22] H.-T. Chou, Y.-T. Hsaio, P. H. Pathak, P. Nepa, and P. Janpugdee, "A fast DFT planar array synthesis tool for generating contoured beams," *IEEE Antennas Wireless Propagat. Lett.*, vol. 3, pp. 287–290, 2004.

[23] Z. Zhang, M. F. Iskander, Z. Yun, and A. Host-Madsen, "Hybrid smart antenna system using directional elements—Performance analysis in flat Rayleigh fading," *IEEE Trans. Antennas. Propag.*, vol. 51, no. 10, pp. 2926–2935, Oct. 2003.

[24] J. Wang, H. Zhu, and N. J. Gomes, "Distributed antenna systems for mobile communications in high speed trains," *IEEE J. Sel. Areas Commun.* vol. 30, no. 4, pp. 675–683, May 2012.

[25] H. Zhu, "Performance comparison between distributed antenna and microcellular systems," *IEEE J. Sel. Areas Commun.*, vol. 29, no. 6, pp. 1151–1163, Jun. 2011.

[26] D. Wang, J. Wang, X. You, Y. Wang, M. Chen, and X. Hou, "Spectral efficiency of distributed MIMO systems," *IEEE J. Sel. Areas Commun.*, vol. 31, no. 10, pp. 2112–2127, Oct. 2013.

[27] A. Papadogiannis, and A. G. Burr, "Multi-beam assisted MIMO-A novel approach to fixed beamforming," in *Proc. Future Netw. Mobile Summit*, 2011, pp. 1–8.

[28] Y. Zheng, G. Hua, H. Zhou, and W. Hong, "Research of multi-beams antenna array using butler matrix in MIMO communication," in *Proc. 3rd Asia–Pacific Conf. IEEE, Antennas Propag*, 2014, pp. 225–227.

[29] Q. L. Luo, F. Pei, J. H. Zhang, and M. Zhang, "3D MIMO channel model based on field measurement campaign for UMa scenario," in *Proc. IEEE Wireless Commun. Netw. Conf.*, Apr. 6–9, 2014, pp. 171–176.

[30] C. A. Balanis, "Antenna synthesis and continues sources" in *Antenna Theory, Anal. Design*, 3rd ed., New York, NY, USA: Wiley, 2005, pp. 393–399.

[31] D. M. Pozar, "Mircowave network analysis" in *Microw. Eng.*, 3rd ed., New York, NY, USA: Wiley, 2005, pp. 177–178.

[32] J. Butler and R. Lowe, "Beam-forming matrix simplifies design of electronically scanned antennas," *Electron. Design*, vol. 9, pp. 170–173, 1961.

[33] S. V. Hum and J. Perruisseau-Carrier, "Reconfigurable reflectarrays and array lenses for dynamic antenna beam control: A review," *IEEE Trans. Antennas. Propag.*, vol. 62, no. 1, pp. 183–198, Jan. 2014.

[34] B. Cetinoneri, Y. A. Atesal, and G. M. Rebeiz, "An $8 \times 8$ butler matrix in 0.13-$\mu$m CMOS for 5-6-GHz multibeam applications," *IEEE Trans. Microw. Theory Tech.*, vol. 59, no. 2, pp. 295–301, Feb. 2011.

[35] 3GPP, "Spatial channel model for multiple input multiple output (MIMO) simulations," 3GPP, Sophia Antipolis Cedex, France, Tech. Rep. TR25.996, V10.0.0, Mar. 2011.

[36] 3GPP, "Study on 3D channel model for LTE," 3GPP, Sophia Antipolis Cedex, France, Tech. Rep. TR36.873, V12.1.0, Mar. 2015.

[37] J. H. Winters, "Optimum combining in digital mobile radio with cochannel interference," *IEEE J. Sel. Areas Commun.*, vol. 2, no. 4, pp. 528–539, Jul. 1984.

[38] A. F. Molisch, "Multinatenna Systems" in *Wireless Commun.*, 2nd ed., New York, NY, USA: Wiley, 2011, pp. 488–490.

[39] C. B. Peel, B. M. Hochwald, and A. L. Swindlehurst, "A vector-perturbation technique for near-capacity multiple-antenna multiuser communication—Part I: Channel inversion and regularization," *IEEE Trans. Commun.*, vol. 1, no. 53, pp. 195–202, Jan. 2005.


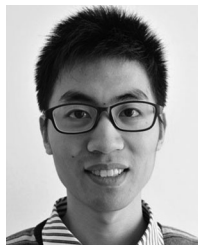

**Xiaolei Jiang** (S'13–M'17) received the B.S. degree in electronics and information engineering in 2011, and the Ph.D. degree, in 2016, both from Tsinghua University, Beijing, China.

He was a Visiting Scholar at Tokyo Institute of Technology, Ando and Hirokawa Lab, Japan, from Oct. 2014 to Mar. 2015. Since July 2016, he has been with Huawei Technologies, Beijing, China, where he is currently a Senior Antenna Design Engineer. He is also a reviewer of the IEEE TRANSACTIONS ON ANTENNAS AND PROPAGATION and the IEEE ANTENNAS AND WIRELESS PROPAGATION LETTERS.

**Han Wang** received the B.S. degree in applied physics from the Beijing University of Posts and Telecommunications, Beijing, China, in 2010, and the Ph.D. Degree in electronic science and technology from Tsinghua University, Beijing, China, in 2015.

His current research interests include antenna design and theory, particularly in mobile/handset antenna, smart antenna, MIMO antenna, wearable antenna, and antenna for IOT devices.

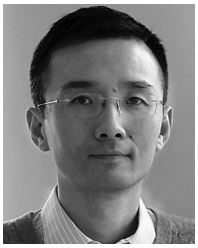

**Zhijun Zhang** (M'00–SM'04–F'15) received the B.S. and M.S. degrees from the University of Electronic Science and Technology of China, Chengdu, China, in 1992 and 1995, respectively, and the Ph.D. degree from Tsinghua University, Beijing, China, in 1999.

In 1999, he was a Postdoctoral Fellow with the Department of Electrical Engineering, University of Utah, where he was appointed a Research Assistant Professor in 2001. In May 2002, he was an Assistant Researcher with the University of Hawaii at Manoa, Honolulu, HI, USA. In November 2002, he joined Amphenol T&M Antennas, Vernon Hills, IL, USA, as a Senior Staff Antenna Development Engineer and was then promoted to the position of Antenna Engineer Manager. In 2004, he joined Nokia Inc., San Diego, CA, USA, as a Senior Antenna Design Engineer. In 2006, he joined Apple Inc., Cupertino, CA, USA, as a Senior Antenna Design Engineer and was then promoted to the position of Principal Antenna Engineer. Since August 2007, he has been with Tsinghua University, where he is a Professor in the Department of Electronic Engineering. He is the author of *Antenna Design for Mobile Devices* (Wiley, 1st ed. 2011, 2nd ed. 2017). He was Associate Editor of the IEEE TRANSACTIONS ON ANTENNAS AND PROPAGATION (2010–2014), and the IEEE ANTENNAS AND WIRELESS PROPAGATION LETTERS (2009–2015).

**Xinyu Gao** (S'14) received the B.E. degree in communication engineering from Harbin Institute of Technology, Heilongjiang, China in 2014. He is currently working toward the Ph.D. degree in electronic engineering from Tsinghua University, Beijing, China. He has published several journal and conference papers in the IEEE JOURNAL ON SELECTED AREAS IN COMMUNICATIONS, the IEEE TRANSACTION ON VEHICULAR TECHNOLOGY, IEEE ICC, IEEE GLOBECOM, etc. His research interests include massive MIMO and mmWave communications, with the emphasis on signal detection and precoding. He received the national scholarship in 2015.

**Linglong Dai** (M'11–SM'14) received the B.S. degree from Zhejiang University, Hangzhou, China, in 2003, the M.S. degree (with the highest honor) from the China Academy of Telecommunications Technology, Beijing, China, in 2006, and the Ph.D. degree (with the highest honor) from Tsinghua University, Beijing, China, in 2011. From 2011 to 2013, he was a Postdoctoral Fellow with the Department of Electronic Engineering, Tsinghua University, where he has been an Assistant Professor since July 2013. He has published more than 50 IEEE journal papers and more than 30 IEEE conference papers. His research interest is wireless communications, with a focus on multicarrier techniques, multiantenna techniques, and multiuser techniques. He has received the Outstanding Ph.D. Graduate of Tsinghua University Award in 2011, the Excellent Doctoral Dissertation of Beijing Award in 2012, the IEEE ICC Best Paper Award in 2013, the National Excellent Doctoral Dissertation Nomination Award in 2013, the IEEE ICC Best Paper Award in 2014, the URSI Young Scientists Award in 2014, the IEEE Transactions on Broadcasting Best Paper Award in 2015, the IEEE RADIO Young Scientists Award in 2015. He currently serves as a Co-Chair of the IEEE Special Interest Group (SIG) on Signal Processing Techniques in 5G Communication Systems.

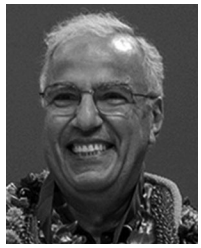

**Magdy F. Iskander** (F'93–LF'12) was a Professor of electrical and computer engineering and the Engineering Clinic Endowed Chair Professor with the University of Utah, Salt Lake City, UT, USA. In 2002, he joined the University of Hawaii at Manoa, Honolulu, HI, USA, where he is currently a Professor of electrical engineering and the Director of the Hawaii Center for Advanced Communications, College of Engineering. He is also the Co-Director of the NSF Industry/University Co-operative Research Center with four other universities. He has authored more than 250 papers in technical journals, holds nine patents, and has made numerous presentations at national/international conferences. He has authored and edited several books, including the textbook *Electromagnetic Fields and Waves* (Prentice Hall, 1992, and Waveland Press, 2001; 2nd ed. 2012), and four books published by the Materials Research Society on Microwave Processing of Materials. His research in computational and biomedical electromagnetics and wireless communications was funded by the National Science Foundation, National Institute of Health, Army Research Office, U.S. Army CERDEC, Office of Naval Research, and several corporate sponsors.

He has received many awards for excellence in research and teaching, including the University of Hawaii Board of Regents Medal for Excellence in Research in 2013, the Board of Regents' Medal for Teaching Excellence in 2010, and the Hi Chang Chai Outstanding Teaching Award in 2011 and 2014, which is based on votes by graduating seniors. He has also received the IEEE MTT-S Distinguished Educator Award in 2013, the IEEE AP-S Chen-To Tai Distinguished Educator Award in 2012, and the Richard R. Stoddard Award from the IEEE EMC Society in 1992. He received the Northrop Grumman Excellence in Teaching Award in 2010, the American Society for Engineering Education Curtis W. McGraw National Research Award in 1985, and the ASEE George Westinghouse National Award for Excellence in Education in 1991. He was the President of the IEEE Antennas and Propagation Society in 2002, a Distinguished Lecturer, and a Program Director of the Electrical, Communications, and Cyber Systems Division at the National Science Foundation. He has been the Founding Editor of the *Computer Applications in Engineering Education Journal* (Wiley), since 1992.